Mechanistic Details of the spontaneous Intercalation of Li metal into Graphite Electrodes

Christin Hogrefe[a], Simon Hein[b,c], Thomas Waldmann[a,*], Timo Danner[b,c], Karsten Richter[a], Arnulf Latz[b,c,d], Margret Wohlfahrt-Mehrens[a,c]

[a] ZSW - Zentrum für Sonnenenergie- und Wasserstoff-Forschung Baden-Württemberg, Helmholtzstrasse 8, D-89081 Ulm, Germany
[b]DLR – German Aerospace Center, Institute of Engineering Thermodynamics, D-70569, Germany
[c]HIU - Helmholtz Institute for Electrochemical Energy Storage, Helmholtzstrasse 11, D-89081 Ulm, Germany
[d]UUlm – Ulm University, Institute of Electrochemistry, D-89081 Ulm, Germany

* Corresponding Author contact
Dr. Thomas Waldmann
ZSW - Zentrum für Sonnenenergie- und Wasserstoff-Forschung Baden-Württemberg, Helmholtzstrasse 8
D-89081 Ulm, Germany
thomas.waldmann@zsw-bw.de
Tel: +49(0)731-9530-212
Fax: +49(0)731-9530-666

Keywords: Lithium-ion cells, graphite electrodes, kinetics, intercalation, pre-lithiation

- Supporting Information -

S1 Details of the electrochemical model

The graphite electrode is modelled as porous, homogeneous medium, similar to porous electrode theory. The transport of Li ions in the electrolyte within the electrode is described by

$$\frac{\partial(\epsilon c_{El})}{\partial t} = -\vec{\nabla} \cdot \vec{N}_{El}^{eff} \quad (1)$$

$$0 = -\vec{\nabla} \cdot \vec{j}_{el}^{eff} \quad (2)$$

With the effective particle flux density N and effective charge flux density J given by

$$\vec{N}_{El}^{eff} = -D_{El}^{eff} \vec{\nabla} c_{El} + \frac{t_{\pm}}{F} \vec{j}_{El}^{eff} \quad (3)$$

$$\vec{j}_{El}^{eff} = -\kappa_{El}^{eff} \vec{\nabla} \varphi_{El} + \kappa_{El}^{eff} \frac{1 - t_{\pm}}{F} \left(\frac{\partial \mu_{El}}{\partial c_{El}} \right) \vec{\nabla} c_{El} \quad (4)$$

Due to the size of the Li disk, the limiting step in the lithiation process is the transfer of Li ions through the electrolyte towards the active material. Therefore, the diffusion of Li inside the graphite particles which happens on much smaller timescales (4 orders of magnitude) is neglected. Still, we keep track of the Li concentration within the Graphite phase according to

$$\frac{\partial c_{So}}{\partial t} = -\vec{\nabla}\vec{N}_{So} \tag{5}$$

Where the transport of Li within the Graphite domain is given by the effective diffusion in the phase

$$\vec{N}_{So} = -D_{So}^{eff}\vec{\nabla}c_{So} \tag{6}$$

The electronic connection between the Li disk and the graphite electrode is critical for the lithiation process. Without electrical contact, charge transfer between Li and graphite is impossible which will stop the dissolution process. In order to keep track of local electrical currents we solve the charge conservation equation inside the solid regions of the model cell:

$$0 = -\vec{\nabla}\vec{j}_{So}^{eff} \tag{7}$$

With the electronic current density given by

$$\vec{j}_{So}^{eff} = \sigma_{So}\vec{\nabla}\Phi_{So} \tag{8}$$

At the interface between the electrolyte and the graphite, the Li de-/intercalation is described by a classical Butler-Volmer expression

$$i_{BV} = i_{00}c_{El}^{\alpha}\, c_{So}^{1-\alpha}\, (c_{So}^{max} - c_{So})^{1-\alpha} \times \left[\exp\left(\frac{\alpha F}{RT}\eta\right) - \exp\left(-\frac{(1-\alpha)F}{RT}\eta\right)\right] \tag{9}$$

with the exchange current density i_{00}, the maximum Li concentration in graphite c_{so}^{max}, the symmetry factor α, and the overpotential η driving the reaction. The overpotential is given by

$$\eta = \Phi_{So} - \varphi_{El} - U_0(c_{So}) \tag{10}$$

The experiments on model electrodes without conductive salt demonstrate that direct intercalation of Li from the disk into graphite is minor. Therefore, we only include de-/intercalation from the electrolyte.

A challenge of simulating the chemical lithiation using a metallic Li disk is the complete dissolution of the metallic Li phase. This kind of extensive volume change is expected to introduce convection into the electrolyte. On the other hand, the chemical lithiation takes place in a long period of time, therefore, it can be expected, that the convection

is negligibly small. In this work, we use a simplified description of the Li disk, where we do not take into account changes of our computational domain during dissolution. Still, we keep track of the amount of Li within the disk by solving the conservation equation for the Li phase:

$$\frac{\partial c_{Li}^{disk}}{\partial t} = -\vec{\nabla}\vec{N}_{Li}^{disk} \tag{11}$$

In this lumped model dissolved Li is immediately replaced by electrolyte. The transport of Li within the domain is then given by effective transport in the electrolyte

$$\vec{N}_{Li}^{disk} = -D_{Li}^{disk}\vec{\nabla}c_{Li}^{disk} \tag{12}$$

Therefore, the effective transport parameter within the Li disk D_{Li}^{disk} is chosen to represent transport inside the electrolyte.

Since we do not change the computational domain, the geometry of the Li disk affects transport in the electrolyte even after the complete dissolution. A similar effect is expected due to the remains of the Li disk observed in the experiments. However, this thinner layer is probably more permeable for Li ions. Therefore, our model assumption probably overestimates this blocking effect where Li ions in electrode pores underneath the disk can only diffuse through the electrode pore space and not towards the counter electrode. The distribution of Li in this region is therefore probably slightly overestimated.

At the interface between the electrolyte and the Li disk the kinetic expression is given by

$$i_{BV} = i_{00}c_{El}^{\alpha}\left[\exp\left(\frac{\alpha F}{RT}\eta\right) - \exp\left(-\frac{(1-\alpha)F}{RT}\eta\right)\right] \tag{13}$$

During the experiment the Li disk is able to completely dissolve. This effect is taken into account through a variation of the activity of the Li metal for vanishing Li content.

$$\eta_{Li-Disk} = \Phi_{Li} - \varphi_{El} + \frac{RT}{F}\ln\left(a_{Li}(c_{Li})\right) \tag{14}$$

As long as the Li concentration is sufficiently large, the activity of bulk Li metal a_{Li} is one by definition. In our model the activity and, thus the corresponding Faradaic current, will approach zero for vanishing amounts of Li.

The Li metal counter electrode serves as a reference in the electrochemical measurements. In the simulations, the counter electrode is modeled as infinite reservoir for Li ions following the kinetic description given in Eq. 9.

The electrochemical parameters for the electrolyte and the graphite are taken from Hein et al.[25] and are listed in Table SI-1. The transport inside the electrolyte phase of the electrode (index *El*) and the long range diffusion within Graphite (index *So*) are reduced according to ϵ^{β} with the corresponding volume fraction of the respective phase and a classical Bruggeman factor $\beta_{So} = \beta_{El} = 1.5$. The volume fraction of the pore space is 30% and the solid fraction of the electrode is 70%. This Bruggeman expression is related to a tortuosity expression according to $\epsilon_i^{\beta_i} = \frac{\epsilon_i}{\tau_i}$. The reaction rate of the Li dissolution reaction at the Li disk together with the diffusion of Li inside the disk describe the Li dissolution process. The value of the diffusion was set to $D_{Li} = 3.8279 \cdot 10^{-4}\ cm^2/s$ and the rate constant was chosen to $i_{00}^{LiDisk} = 0.002511886 \frac{A}{\sqrt{cm\ mol}}$ in order to qualitatively reproduce the dissolution process.

The open circuit voltage of Graphite is given by the following equation:

$$U_0(x) = 0.6379 + 0.5416 \cdot \exp(-305.5309 \cdot x) + 0.044 \cdot \tanh\left(-\frac{x - 0.1958}{0.1088}\right) - 0.1978 \cdot \tanh_{\mathrm{mod}}\left(\frac{x - 0.99}{0.05}\right) - 0.6875 \cdot \tanh\left(\frac{x + 0.0117}{0.0529}\right) - 0.0175 \cdot \tanh\left(\frac{x - 0.5692}{0.0875}\right) \quad (15)$$

$$\tanh_{mod}(x) = \frac{\exp(20 \cdot x) - \exp(-x)}{2 \cdot \cosh(x)}$$

The expression is based on the work of Safari et al. [SI-2].

Table S1: List of the electrochemical parameters used for the simulations.

Parameter	Value	Description
Graphite		
c_{So}^0 / mol/cm³	3.137e-6	Initial Li concentration
c_{So}^{max} / mol/cm³	31370e-6	Maximum Li concentration [SI-2]
D_{So} / cm²/s	3e-10	Li ion diffusion coefficient [SI-2]
κ_{So} / S/cm	10	Electronic conductivity of Graphite (estimated)

U_0 / V	See Ref. 13	Open circuit potential of Graphite
Electrolyte		
c_{El}^0 / mol/l	1	Concentration of Li salt
κ_{El} / S/cm	Eqn (4) in [SI-1] based on [SI-3]	Conductivity
D_{El} / cm^2/s	Eqn (3) in [SI-1] based on [SI-3]	Li ion diffusion coefficient
f_{Li}^{Elyte} / -	Eqn (3) in [SI-1] based on [SI-3]	Activity factor
$t_{\pm}$ / -	Eqn (2) in [SI-1] based on [SI-3]	Transference number
κ_{CC} / S/cm	10	Electronic conductivity of Current collector (estimated)
D_{Li} / cm^2/s	3.8279e-4	Li “diffusion coefficient” inside Li disk (model parameter)
Kinetic parameter		
i_{00}^{CE} / A/cm^2	0.0364	Exchange current density factor at counter electrode [SI-1]
i_{00}^{Li} / Acm$^{1.5}$/mol$^{0.5}$	0.002511886	Exchange current density factor at Li disk (model parameter)
i_{00}^{So} / Acm$^{2.5}$/mol$^{1.5}$	0.0657	Exchange current density factor for intercalation[SI-2]
Geometrical parameter		
A / cm^2/cm^3	1.125e3	Specific surface area of Graphite electrode (calculated)

[SI-1] L. S. Kremer et al., “Manufacturing Process for Improved Ultra-Thick Cathodes in High-Energy Lithium-Ion Batteries,” Energy Technol., 8, 1900167, (2020).

[SI-2] M. Safari and C. Delacourt, “Modeling of a Commercial Graphite/LiFePO4 Cell,” J. Electrochem. Soc., 158, A562–A571 (2011).

[SI-3] A. Nyman, M. Behm, and G. Lindbergh, “Electrochemical characterisation and modelling of the mass transport phenomena in LiPF6-EC-EMC electrolyte,” Electrochim. Acta, 53, 6356–6365 (2008).

S2 Simulations with reduced counter electrode

In the experiments, we observe a complete dissolution of the Li metal disk in a setup with counter electrode, which was introduced for OCP measurements. This is not seen in experiments without the additional counter-electrode. The influence of the geometry of the counter electrode is also investigated by one additional simulation. The simulation domain with a reduced counter electrode can be seen on the left side of Figure S1. The counter electrode is reduced to a fraction of the size and is located at the bottom of the pouch cell. This setup is similar to the experiments without counter-electrode. Still, we are able to additionally simulate the corresponding OCP which is not tracked in the experiments. The electrochemical simulations reveal, that the cell potential decreases slower compared to the large counter electrode. This is the result of the reduced dissolution of the Li disk. This supports our claim, that the extended counter electrode enhances the Li dissolution. In Figure S2, the Li ion concentration in the electrolyte right next to the counter electrode in both cases are shown. The location of the Graphite electrode and its current collector, roughly 290 µm and 350 µm below the shown slice, are schematically shown in the first image on the left. When Li is dissolving, it is reflected by the increased Li concentration in the electrolyte. Without the metallic Li counter facing the surface, only at the position close to the Li metal disk, an increase of Li ion concentration can be observed. Remarkably, this concentration can reach up to 3 mol/l and consequently we also observe concentrations lower than the initial salt concentration away from the Li disk. In the lower panel, with the additional diffusion/reaction path given by the large counter electrode, the increase in Li ion concentration can not only be seen at the Li metal disk but also at the edges of the electrode. Therefore, the counter-electrode accelerates redistribution of the Li ions in the electrolyte. The asymmetric concentration profile is caused by the asymmetry in cell setup due to the current collectors. The current collector is blocking the electrolyte transport on the top right which causes an inhomogeneous transport and Li concentration distribution. This can be seen in the first image of the lower row in Figure S2 and the shape and position of the electrode and current collector is indicated by the black mesh. Since, high concentrations also reduce dissolution kinetics this

phenomenon is responsible for the residual Li disk in the experiments without counter electrode. Due to this additional diffusion path, equilibration of Li ions in the electrolyte can be achieved within 700 h, whereas no equilibrium is reached when the Li metal counter electrode is not facing the graphite electrode.

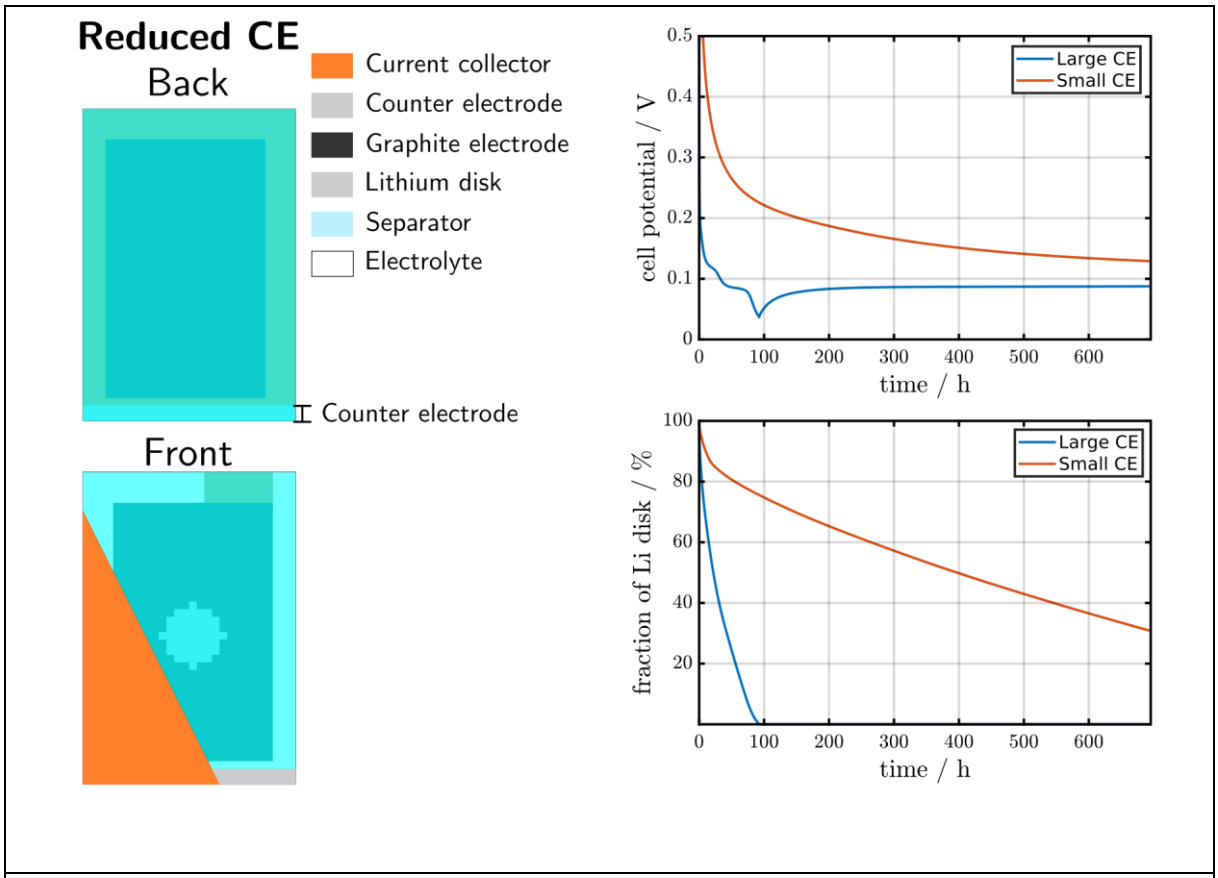

Figure S1: (left) Geometry of the pouch cell with a reduced counter electrode, which is located on the bottom. (right top) The cell potential of the small counter electrode exhibits exponential behavior. (right bottom) The remaining amount of Li in the Li disk. The small CE leads to a slower dissolution of the Li disk.

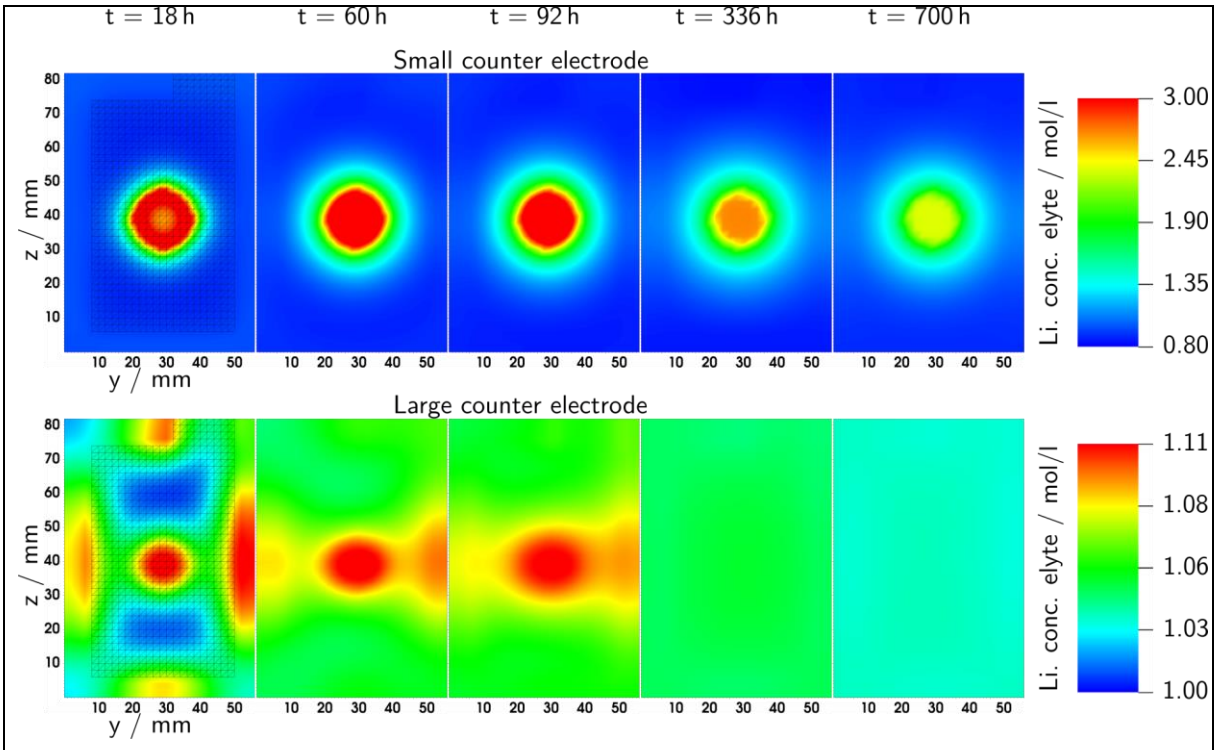

Figure S2: Li ion distribution in the electrolyte right next to the counter electrode during the dissolution and re-intercalation (upper panel) with no metallic Li counter electrode facing the graphite electrode surface (lower panel) with a metallic Li counter electrode facing the graphite electrode surface. The black mesh indicates the shape and position of the electrode and current collector.